

V2324 Cyg – an F-type star with fast wind

V.G. Klochkova, E.L. Chentsov & V.E. Panchuk

Special Astrophysical Observatory RAS, Nizhnij Arkhyz, 369167 Russia

November 8, 2018

Abstract For the first time high-resolution optical spectroscopy of the variable star V2324 Cyg associated with the IR-source IRAS 20572+4919 is made. More than 200 absorption features (mostly Fe II, Ti II, Cr II, Y II, Ba II, and Y II) are identified within the wavelength interval 4549–7880 Å. The spectral type and rotation velocity of the star are found to be F0 III and $V \sin i = 69$ km/s, respectively. H I and Na I D lines have complex P Cyg-type profiles with an emission component. Neither systematic trend of radial velocity V_r with line depth R_o nor temporal variability of V_r have been found. We determined the average heliocentric radial velocity $V_r = -16.8 \pm 0.6$ km/s. The radial velocities inferred from the cores of the absorption components of the H β and Na I wind lines vary from -140 to -225 km/s (and the expansion velocities of the corresponding layers, from about 120 to 210 km/s). The maximum expansion velocity is found for the blue component of the split H α absorption: 450 km/s for December 12, 1995. The model atmospheres method is used to determine the star's parameters: $T_{eff} = 7500$ K, $\log g = 2.0$, $\xi_t = 6.0$ km/s, and metallicity, which is equal to the solar value. The main peculiarity of the chemical abundances pattern is the overabundance of lithium and sodium. The results cast some doubt on the classification of V2324 Cyg as a post-AGB star.

1. Introduction

The poorly studied star V2324 Cyg (visible magnitude $V = 11^m.63$, color indices $B - V = +1^m.09$ and $U - B = +0^m.58$, and galactic coordinates $l = 89^\circ.44$, $b = 2^\circ.39$) is an optical counterpart of the IR-source IRAS 20572+4919. The observed 12–60 μm flux of the star and its location on the IR color-color diagram suggest that this object is a candidate young planetary nebula with a dust envelope [1].

According to current theories (see, e.g., [2]) objects observed during the short-lived evolutionary stage of young planetary (protoplanetary) nebulae (pPN) are intermediate-mass stars evolving off the asymptotic giant branch (AGB) toward the planetary nebula phase. The initial mass of these stars lies in the interval $3 - 8 M_\odot$. During the preceding AGB stage these stars have undergone essential mass loss in the form of powerful stellar wind, so that the resulting protoplanetary nebula has the form of a degenerate carbon-oxygen core with a typical mass of about $0.6 M_\odot$ surrounded by an expanding gas-and-dust envelope. The astronomers' interest toward pPN is due, first, to the fact that these objects

opportunity to observe the result of stellar nucleosynthesis, mixing, and dredge-up of the products of nuclear reactions during the previous evolution of the star.

The particular attention of the astronomers towards pPN over the past decade yielded a number of interesting results. The sample of pPN candidates was found to contain about a dozen objects overabundant in heavy metals synthesized via neutronization of iron nuclei under conditions of low neutron density (*s*-process). The physical conditions necessary for efficient *s*-process and subsequent dredge-up of the matter enriched in heavy nuclei can be found just in stars at the AGB stage (for the history and modern understanding of the problem see the review by Busso et al. [3]). An analysis of the spectra of the sample of pPN objects showed that the expected overabundances of *s*-process elements are observed in the atmospheres of those pPN stars whose atmospheres are carbon enriched and whose IR spectra exhibit an emission at $21\ \mu\text{m}$ [4, 5, 6, 7]. The overwhelming majority of pPN stars exhibit neither carbon (O-rich stars), nor heavy-metal overabundance (see, e.g., [4, 8, 9]). The correlation found between the overabundance of heavy metals in the star atmosphere and the peculiarities of the IR spectrum of the star envelope should be explained, hence the sample of well-studied pPNe should be extended.

We know little about the properties of the star V2324 Cyg. Arkhipova et al. [10, 11] performed long-term UBV observations and found V2324 Cyg to be variable with an amplitude of about $0^{\text{m}}3$ in the U band and about $0^{\text{m}}2$ in the V and B bands. The conclusion made by Arkhipova et al. [11] about the absence of well-defined pulsation periodicity in the star’s light variations is of great importance. The above authors explain the photometric variability of the star by the effect of the stellar wind. The lack of pulsations was found to be consistent with the rather early spectral type of the star – A3I [11]. Note that SIMBAD lists a different spectral type – Sp = Fe. In the polarimetric survey [12] the source IRAS 20572+4919 is classified as an object without polarization, and this fact may be indicative of a spherical shape of the circumstellar shell. Hrivnak et al. [13] analyzed near-IR spectra of a sample of pPN objects and pointed out the anomalous (flat) form of the IR spectrum and the lack of Brackett hydrogen lines in the spectrum of IRAS 20572+4919. Kelly and Hrivnak [14], in their near-IR study of the pPN sample in the $2.1\text{--}2.3\ \mu\text{m}$ wavelength interval, classified the central star of the source as an F-type star and put it among the small group of stars with a $\text{Br}\gamma$ emission. Garcia-Lario et al. [15], who used IR photometry to determine the evolutionary status of 225 IRAS sources, consider the classification of the IRAS 20572+4919 source as a “post-AGB” star to be tentative.

So far only low-resolution optical spectroscopy was performed for V2324 Cyg, however, even low-resolution observations revealed the main peculiarities of the optical spectrum of V2324 Cyg – NaI D-line emission and especially powerful emission in $\text{H}\alpha$. The $\text{H}\alpha$ emission was found more than 30 years ago [16]. Emission is naturally associated with the presence of a circumstellar shell, which affects $\text{H}\alpha$ and NaI D-line profiles in the optical spectrum. Recently, a 2\AA -resolution spectrum of V2324 Cyg has been published [17], which shows, in particular, the presence of emission in the lines of the $\text{OI}\ \lambda\ 7773\ \text{\AA}$ triplet.

In this paper we present the results of a spectroscopic monitoring of V2324 Cyg with high spectral resolution performed with the 6-m telescope of the Special Astrophysical Observatory of the Russian Academy of Sciences (SAO RAS). The aim of our study is to detect the spectroscopic variability, analyze the velocity field in the atmosphere and envelope of the star, determine the fundamental parameters, metallicity and chemical

the methods of observation and data reduction; in Section 3 we reports and analyzes the results obtained, and finally in Section 4 we briefly formulates the main conclusions.

2. Observations and data reduction

Our observations of V2324 Cyg were performed with the 6-m telescope of the SAO RAS. The first spectrum was taken in 1995 with a spectroscopic resolution of $R=25000$ with the Lynx—echelle spectrograph [18] mounted in the Nasmyth focus. PFES combined with a $1K \times 1K$ CCD, recorded the wavelength interval $\lambda\lambda$ 4720–6860 Å. The second spectrum was taken with the Primary Focus Echelle Spectrograph PFES [19] ($R = 15000$). This spectrograph, combined with a $1K \times 1K$ CCD, recorded the wavelength interval $\lambda\lambda$ 4680–8590 Å. All the subsequent observations of the star we made in the Nasmyth focus with NES echelle spectrograph [20], which provides a spectral resolution of $R=60000$. Observations were performed using a large-format 2048×2048 CCD and with an image slicer [20]. Table 1 lists the following data for each spectrum: date, average UT observing time, integration time, wavelength interval, and the spectrograph employed.

We extracted the data from the two-dimensional echelle spectra using the modified [21] context of MIDAS package. Cosmic-ray hits were removed via median averaging of two spectra taken consecutively one after another. Wavelength calibration was performed using the spectra of a hollow-cathode Th-Ar lamp. To perform subsequent reduction including spectrophotometric and position measurements we used DECH20 [22] program.

3. Discussion of results

3.1. Peculiarities of the optical spectrum of V2324 Cyg

We obtained most of our spectroscopic data described in Table 1 with the limiting spectral resolution $R \approx 0.1$ Å. Even a preliminary examination of the high-resolution spectra showed that V2324 Cyg is an F-type star with wide absorptions and P Cyg-type profiles for some lines (in the recorded wavelength interval these are $H\alpha$, $H\beta$, D1 and D2 NaI lines). Besides the expected emissions in $H\alpha$ and in the lines of the NaD doublet, we found another spectral peculiarity – the large widths of absorption lines, which is untypical for a star with the post-AGB status.

Spectral type. Arkhipova and Ikonnikova [10] obtained an indirect estimate of the star’s spectral type, B8–A2 Ib–II, based on the results of photometric observations. Pereira and Miranda [17] found a later spectral type from a low-resolution spectrum, but report equally high luminosity. The above authors chose the HD 842 star (an A9 I-type supergiant) from the atlas of Jacoby et al. [23] to be closest to V2324 Cyg in terms of spectrum. However, the classification of V2324 Cyg given by Pereira and Miranda [17] is not satisfactory for two reasons:

1. The spectrum of V2324 Cyg reported by Pereira and Miranda [17] is also very similar to another spectrum of atlas of Jacoby et al. [23] – that of HD 64191 F0-3 III (the δ Sct-type variable AD CMi). The depth ratio of the G-band to $H\gamma$ allows V2324 Cyg to be classified even as an F5-type star, however, below we show that Balmer lines in the spectrum of V2324 Cyg are anomalous.

2. The result of classification may be distorted by the widths of absorptions [24] which

V2324 Cyg, HD 842, and HD 64191 are equal to 69 km/s (as measured from our spectra), 16 km/s (also our estimate, but based on a spectrum adopted from ELODIE.3 [25] and ELODIE.3.1 [26] libraries), and 12 km/s [27], respectively.

Our data allowed us to perform spectral classification based on line intensity ratios of neutral to ionized atoms. We primarily used numerous FeI and some of the FeII absorptions. To build the calibration curves, we used the data from the atlas of Klochkova et al. [28] and ELODIE.3 spectral libraries [25]. The latter paper is especially convenient for us because it contains spectra with the lines of approximately the same width as those in the spectrum of V2324 Cyg and we can directly compare their fragments and profiles of lines and blends and compare the line depths rather than the equivalent widths.

Within the spectral type F absorption depth ratios in the FeII/FeI line pairs decrease from F0 to F8 and they are higher and decrease more abruptly for supergiants than for main-sequence stars. The depth ratios for V2324 Cyg correspond to a spectral type interval from A9–F0 V to F8–G0 I. The supergiant option must be rejected, because it would imply too large line depths for the depth ratios in question.

The spectra of ELODIE.3 library [25] for stars with rotation velocities in the 60 to 80 km/s interval – HD 58923 (F0 III), HD 47072 (F0 II), HD 432 (F2 III(IV)), and HD 219877 (F3 IV) – reproduce our spectra of V2324 Cyg fairly well. The above stars have bona fide parallaxes (ranging from 9 to 60 mas according to HIPPARCOS catalog) and direct estimates of their absolute magnitudes yield $0.2 < M_v < 2.8^m$. These estimates are consistent with the MK spectral types for the three stars and the only exception is HD 47072 whose parallax is indicative of a III–IV luminosity class.

A comparison of the mean central depths R_o of absorption lines averaged over the spectra of the comparison stars mentioned above with the mean depths averaged over our spectra of V2324 Cyg show that, with a few strongest lines excluded, these averaged R_o agree within errors to both for FeI and FeII. It is thus safe to assume that V2324 Cyg is an early F-type giant or subgiant. We estimate the spectral type more accurately by analyzing the dependences of the $R_o(\text{FeII})/R_o(\text{FeI})$ ratios on spectral type Sp obtained for stars of luminosity classes III and IV. Thus, e.g., the depth ratio for the pair of closely located lines FeII(43) λ 4732 and FeI(554) λ 4737 decreases from 1.3 to 0.9, and that for the FeII(40) λ 6433, FeI(62) λ 6431 blend, from 1.6 to 0.7 as one passes from F0 III to F5 III. The corresponding ratios for V2324 Cyg are equal to 1.05 and 0.98, respectively. Based only on moderate-intensity metal lines, we estimate the spectral type of V2324 Cyg to be F2 III.

Spectral anomalies. Some of spectral features make V2324 Cyg differ markedly from a common early F-type giant. These are, first and foremost, emissions in a number of lines. In the wavelength interval accessible for us such emissions can be directly seen in H α (see Fig. 1) and in the NaI(1) doublet as red shifted components of their P Cyg-type profiles (see Fig. 2). The peaks of emissions in NaI lines are cut by absorptions, however, we can adopt $r \approx 1.25$ as the lower limit of residual intensity for D2 (Fig. 2). It follows from Fig. 1 that the peak of H α emission in our spectra is higher than the continuum level at least by a factor of three (and in two spectra, at least by a factor of four). A comparison of H α profiles in spectra taken at different times is indicative of their variability: both the shape and intensity of emission vary from one spectrum to another and so do the positions of

The $H\beta$ also has a weak emission component whose intensity and position vary with time (see Fig. 3). The presence of emission shows up in the asymmetry of the profile. If we cut the profile into two parts by the vertical line $V_r = 0$, then its red part is raised and the blue part, on the contrary, depressed. At $V_r \approx 100$ km/s the depth of the profile $R \approx 0.1$ – 0.2 , and on August 20, 2003 it even reached the continuum level. At the same time, the blue shifted core of absorption at $V_r \approx -(100$ – $200)$ km/s is deeper than the corresponding feature in the spectra of any comparison star mentioned above (June 12, 2001 $R_o \approx 0.85$).

The OI(1) $\lambda 7774$ blend in the low-resolution spectrum of Pereira and Miranda [17] appears as emission, which is at least comparable to NaI(1) doublet in terms of intensity. In our only spectrum taken on January 12, 2001 the OI(1) $\lambda 7774$ blend also appears to be partly filled by emission: the equivalent width of the blend is $W \approx 0.4$ Å, which, according to Faraggiana et al. [29] corresponds to luminosity class V for early F-subtypes and is twice lower than for an average F2 III-type star.

Moreover, as we pointed out above, for comparing the depths of metal absorption lines in the spectra of V2324 Cyg and those of comparison stars we discarded the strongest lines – first and foremost the FeII(42) and MgI(2) triplets. The average central depths R_o for the comparison stars are ≈ 0.3 , whereas for V2324 Cyg $R_o(\text{FeII}) \approx 0.12$ and $R_o(\text{MgI}) \approx 0.16$. Almost all these lines are parts of close blends and dominate in these blends in the spectra of normal stars. However, in the spectrum of V2324 Cyg these lines are weakened and reduced to the level of other contributors (mostly FeI). We may try to attribute these weaker intensities to the presence of emissions, however, this hypothesis fails to explain why reduced intensity of the lines considered does not result in appreciable blueshifts of FeII(42) and MgI(2) absorptions relative to weak and intermediate metal lines (like in the case of the OI(1) triplet and in contrast to $H\beta$).

3.2. Radial velocities

The velocities that we discuss below are measured only from minimally blended lines. Table 2 lists the main and in some cases also the blending components for these lines, their central residual intensities r , and heliocentric radial velocities V_r .

We found no significant date-to-date variations of the depths and velocities for selected weak and intermediate (photospheric) absorptions. We cannot rule out low-amplitude velocity variations (at a level of 1–2 km/s), but these variations may also be due to pulsations, binarity, or unaccounted systematic measurement errors. Therefore in Table 2 we list for these stars only the mean V_r values averaged over the entire observational data. For the $H\beta$, NaI(1), and $H\alpha$ lines, which exhibited profile variability, Table 2 gives the r and V_r values for each observing date. For the latter two lines the “/” sign separates the quantities corresponding to the absorption and emission components of their P Cyg-type profiles.

The depths of selected photospheric absorptions in Table 2 lie in the interval $0.20 < R_o < 0.03$. Radial velocity V_r does not exhibit appreciable systematic variation with line depth R_o , thereby justifying the computation of the mean velocity $V_r = -16.8 \pm 0.6$ km/s. This velocity must be close to the systemic velocity of the star, V_{sys} . No reliable determination of systemic velocity V_{sys} is available for V2324 Cyg, because no CO

Velocities inferred from the cores of the absorption components of the wind lines vary with time. As is evident from Table 2, in the spectra containing H β and NaID2 the absorption cores of these two lines yield close velocities, which vary from -140 to -225 km/s (and the expansion velocities of the corresponding layers, from about 120 to 210 km/s). The cores of H α lines yield lower radial velocities: they vary from -180 to -280 km/s. The highest expansion velocity (in the spectral domain recorded in our observations) is estimated from the blue boundaries of H α absorptions: it was as high as 450 km/s for the blue component of split absorption measured on December 12, 1995.

3.3. Parameters and chemical composition of the atmosphere

Determination the fundamental parameters from spectroscopic data and of the elemental abundances are difficult to perform in case of V2324 Cyg because of the large width of absorptions in its spectrum caused by large rotation velocity $V \sin i = 69$ km/s. Below we show that the errors of measured equivalent widths are the main contributors to the uncertainty of the chemical composition.

We use the grid of model hydrostatic and LTE atmospheres for different metallicity values computed by Shulyak et al. [32] to determine the parameters of the star's model atmosphere – effective temperature and surface gravity – needed to compute the chemical composition and synthetic spectra. Fixing the main parameters – effective temperature T_{eff} and surface gravity $\log g$ – is known to be always the most difficult part of the computation of the chemical composition of a star. It is difficult to use the photometric data for the finding the effective temperature for objects with uncertain evolutionary status and hence with uncertain reddening. As we noted above, the H I Balmer-line profiles in the spectrum of V2324 Cyg are distorted by variable emission. That is why we determined the effective temperature of the star from the condition that Fe I abundance must be independent on the excitation potential of the corresponding lines; chose the surface gravity based on the condition of ionization balance for iron atoms and ions. The microturbulence velocity ξ_t was determined from the condition that iron abundance must be independent of line intensity. Because of the likely distortion of metal line profiles due to emission, for the above procedures we selected only the lines, where such distortions were visually small or lacking.

The validation criterion for the method is the lack of the dependence of the abundance on the excitation potential of the corresponding lines for other chemical elements represented by numerous lines (Sc II, Ti II, Cr II). Moreover, in the case of a bona fide values of the microturbulence velocity individual abundances must be independent on the equivalent widths of the lines used in the computation. The typical accuracy of model parameters for a star with effective temperature of about 7500 K is $\Delta T_{eff} \approx 200$ K, $\Delta \log g \approx 0.5$ dex, and $\Delta \xi_t \approx 1.0$ km/s. Table 3 lists the abundance errors due to the parameter errors mentioned above. From a comparison of the errors in Tables 3 and 4 one can see that the errors of equivalent line width measurements are the main contributors to the uncertainties for the most abundances.

The known test for the internal consistency of the inferred parameters consists in an agreement between the observed and synthetic spectra. We compared the observed spectrum with the synthetic spectrum that we computed using the code of Shulyak et al. [32]. For computations we adopted the model atmosphere with solar chemical composition and

son of the observed and theoretical spectra (see examples in Figs. 4 and 5) demonstrates their satisfactory agreement provided that we neglect HeI lines and the FeII(42) and MgI(2) lines mentioned above, which are distorted by emission.

We adopted the oscillator strengths $\log gf$ and other atomic constants required for computing the elemental abundances from VALD database [33, 34]. Table 4 lists the adopted parameters of the model atmosphere $T_{eff} = 7500$ K, $\log g = 2.0$, $\xi_t = 6.0$ km/s. We used the solar chemical composition, with respect to which we compute the elemental abundances of the star under study, from Asplund et al. [35]. We performed all our chemical composition computations using the software developed by Shulyak et al. [32] and adapted by the same authors to PCs operating under OS Linux. We computed plane-parallel LTE models using the software described by Shulyak et al. [32] without hyperfine structure and isotopic-shift corrections, which increase the widths of NiI and BaII lines.

The scatter of the elemental abundances inferred from the set of spectral lines is rather small: the standard deviation σ does not exceed 0.3 dex (see Table 4). We determined the parameters of the model atmosphere using only low and intermediate intensity lines with equivalent widths $W \leq 0.25 \text{ \AA}$, because the approximation of a state plane-parallel atmosphere may inadequately describe the strongest spectral features. Moreover, some of the strong absorptions in the spectrum could be distorted by the effect of the circumstellar shell. In the case of insufficient resolution the intensities of the shell components add up to the intensities of the components that form in the atmosphere. We computed the elemental abundances for an extended set of spectral lines – for a number of elements (SiII, TiII, FeI, FeII, BaII) we used lines with equivalent widths exceeding the equivalent-line width limit mentioned above. Let us now analyze the chemical abundances by grouping elements according to the type of their synthesis.

Light elements. As one might expect in the case of an evolved star, the abundances of a number of light elements have changed. The overabundance of lithium computed from the LiI line $\lambda 6707 \text{ \AA}$ is immediately apparent. The equivalent width of this line was measured with confidence in all our spectra of V2324 Cyg and its averaged equivalent width is $W \geq 50 \text{ m\AA}$. We therefore consider the lithium overabundance $[\text{Li}/\text{Fe}] \geq +0.68$ to be established beyond doubt. Figure 6 compares the observed and synthetic spectra of the star in the region of the LiI 6707 \AA line. We performed this computation with the model-atmosphere parameters $T_{eff}=7500$ K, $\log g=2.0$, and $\xi_t=6.0$ km/s and the elemental abundances listed in Table 4. This is the most interesting anomaly in the chemical abundances pattern in the atmosphere of V2324 Cyg.

We find a small underabundance of oxygen $[\text{O}/\text{Fe}] = -0.12$ combined with a small overabundance of carbon $[\text{C}/\text{Fe}] = +0.35$, implying an abundance ratio $\text{C}/\text{O} > 1$. Unfortunately, the OI $\lambda 5330.7$, 6155.9 , and 6158.1 \AA oxygen lines employed are too weak and have their equivalent widths determined with large errors because of the large widths of these lines (in Table 4 the standard error for oxygen is $\sigma = 0.28$). Therefore the inferred oxygen abundance is uncertain. No nitrogen lines were available in the wavelength interval covered by our observations and nitrogen abundance is of fundamental importance for the determination of the evolutionary stage of the star. On the whole, concerning the CNO triad the only certain result is the overabundance of carbon.

The sodium abundance was determined from the moderate intensity NaI $\lambda 5682$, 5688 , and 6160 \AA lines with small NLTE corrections [36, 37]. Hence the sodium overabundance found $[\text{Na}/\text{Fe}] = +1.04$ may be mostly due to the sodium synthesis in the

The magnesium, whose abundance we determined from the two lines, MgI λ 4702.99 and 5528.40 Å, is also overabundant: [Mg/Fe]=+0.43. The sodium-to-magnesium abundance ratio is [Na/Mg]=+0.61.

Iron-peak elements. The iron abundance, which is usually employed as the metallicity indicator, does not differ in the atmosphere of V2324 Cyg from the corresponding solar abundance: $\log \varepsilon(\text{FeI, FeII})=7.44$. The reliably enough determined abundances of chromium and nickel, which belong to the iron group, also differ only slightly from the normal values: [CrI,CrII, NiI/Fe]=−0.19. The solar metallicity of the star is consistent with the systemic heliocentric velocity adopted in Section 2.2, $V_{\odot} \approx -17$ km/s, which is typical of Galaxy disk stars.

Heavy metals. The overabundance of barium with respect to iron, [Ba/Fe]=+0.46, is something expected, but rarely found in the atmospheres of post-AGB supergiants. It is much more common for atmospheres of these stars to exhibit overabundance of *s*-process elements [5, 38]. However, we found no overabundance of yttrium, which is also synthesized via slow neutronization. The overabundance of *s*-process elements or lack of such overabundance depend on the initial mass of the star and on the mass-loss rate at the AGB stage, which determine the evolution of the particular star and the mass of the stellar core. Modeling of the third dredge-up process [39] shows that the efficiency of the dredge-up of reaction products increases with the mass of the core (and hence with the initial mass) of the post-AGB star. It also follows from Herwig’s computations [40] that the efficiency of the dredge-up increases if we take into account penetrative convection at the base of the convective zone.

Separation of chemical elements in the shell. As is well known, selective separation of chemical elements in stars with gaseous-dusty shells may be an efficient mechanism producing anomalous elemental abundances. However, the solar iron abundance for V2324 Cyg indicates that no condensation onto dust grains occurs in this shell, since iron is an element that condenses efficiently onto dust grains. Further evidence is provided by the normal zinc abundance, [Zn/Fe]=+0.09, which is consistent with the typical zinc abundance [Zn/Fe]=+0.04 over a wide range of metallicities [41]. The lack of manifestations of selective separation is difficult to explain for a star with IR excess due to the circumstellar shell.

Related objects. Earlier studied objects include pPN candidates with a chemical composition pattern similar to that found for V2324 Cyg. Arellano-Ferro et al. [42] analyzed a sample of post-AGB stars and found one of them—the hot star HD 172481 (IRAS 18384–2800)—also to be overabundant in lithium. The main parameters of this star— $T_{eff} = 7250$ K and $\log g = 1.5$ —are also similar to those of V2324 Cyg. However, the atmosphere of V2324 Cyg, unlike that of HD 172481, is overabundant with heavy metals. Moreover, Reyniers and Van Winckel [43] suspected that HD 172481, unlike V2324 Cyg, is a binary system and hence the two stars cannot be considered to be full analogs.

All parameters considered, the F-type star HD 331319 (the optical component of the IRAS 19475+3119 source) is a closer analog of V2324 Cyg. This F-type star has close to solar metallicity, it is overabundant in helium, oxygen, and light metals (Na, Si), while being underabundant in titan and barium [8]. Like in the case of V2324 Cyg, the atmosphere of HD 331319, with $T_{eff} = 7200$ K and $\log g = 0.5$, is overabundant in lithium [Li/Fe]=+0.62. It is interesting that Klochkova et al. [8] detected a HeI λ 5876 Å line with the equivalent width of $W_{\lambda} \approx 38$ mÅ in the spectrum of the F-supergiant HD 331319 and

synthesis have been dredged up during the evolution of the star. As for V2324 Cyg, we cannot rule out that the HeI λ 5876 Å line may also be present in its spectrum, at least at some observations. As one can see from Figure 4, where we compare the HeI λ 5876 Å line in the spectrum of V2324 Cyg taken on June 12, 2001 with the synthetic spectrum computed with parameters $T_{eff}=7500$ K, $\log g=2.0$, $\xi_t=6.0$ km/s, the above situation is possible. Neither of these two stars exhibits manifestations of selective separation of chemical elements [42, 8].

However, despite their close effective temperatures, metallicities, and details of chemical composition, V2324 Cyg and HD 331319 differ substantially in luminosity and rotation velocity. Metal lines in the spectrum of HD 331319 are narrow and the star is of luminosity class Ib, whereas lines in the spectrum of V2324 Cyg are broadened by rotation and it is most likely of luminosity class III. The H α profiles in the spectra of these two stars also differ significantly. The H α profile in the spectrum of HD 331319 is typical of post-AGB stars (see Fig. 1 in paper [8]), whereas the P Cyg-type profile of the H α line in the spectrum of V2324 Cyg is closer to the corresponding profiles in the spectra of supergiant stars. Recall that V2324 Cyg has a very high mass outflow velocity – it amounts to several hundred km/s, which is one order of magnitude higher than the typical expansion velocities of pPN envelopes.

There is another pPN candidate, which resembles V2324 Cyg in terms of spectral peculiarities and chemical composition. We mean the spectroscopic binary BD+48°1220 which is the optical component of the IR-source IRAS 05040+4820. The variability of the spectrum of this star has been recently discovered by analyzing the spectra obtained with the 6-m telescope [44], and parameters and chemical composition for this star were determined later [45]. Besides their close temperatures and abundances of a number of chemical elements (solar metallicity, overabundance of lithium and sodium), the similarity of BD+48°1220 and V2324 Cyg also shows up in the variability of profiles of metal lines, which contain an emission component, and in the strong emission in the H α line. The hypothesis that BD+48°1220 and V2324 Cyg may be at close evolutionary stages is also corroborated by the lack of spectral features in their radio spectra. However, these two stars have a very important difference, namely, spectral classification gives the luminosity class Ib for BD+48°1220. The surface gravities inferred via the method of model atmospheres also differ: $\log g=2.0$ and 0.0 for V2324 Cyg and BD+48°1220, respectively.

3.4. The problem of luminosity and evolutionary status of V2324 Cyg

Kinematic distance determinations in the direction of V2324 Cyg ($l \approx 89^\circ 4$, $b \approx 2^\circ 4$) are unreliable: radial velocity slightly depends on distance at least up to 2 kpc [46]. However, color excess and equivalent widths of NaI(1) and DIB interstellar absorptions (see Table 5) exhibit well defined increasing with distance already within the local arm. Both parameters are appreciably smaller for V2324 Cyg than for the members of the large Cyg OB7 association the star projects on and which, according to Humphreys [47], is located at a heliocentric distance of 0.8 kpc. A coarse estimate based on the above parameters yields for V2324 Cyg a distance of $d=0.5-0.6$ kpc, implying a low luminosity of $M_v \approx 1^m 6$. Spectrophotometric estimation based on our spectral type (F2III) and photometry by Arkhipova and Ikonnikova [10] ($V=11^m 7$ and $B-V=1^m 1$) yields an even smaller distance, $d=0.35-0.4$ kpc. Such a low luminosity is also indicative of the low initial mass of

Straniero et al. [48], lithium overabundance may arise during the evolution of the most massive AGB stars with initial masses $\mathcal{M} \approx 7\mathcal{M}_{\odot}$.

However, lithium overabundance in the atmosphere of a low-luminosity star suggests us an alternative evolutionary stage for V2324 Cyg. While analyzing possible mechanisms of lithium enrichment of the Galactic interstellar medium, Romano et al. [49] focus attention on the phenomenon of overabundance of Li in the atmospheres of F-type giants with IR excesses. Some of these Li-rich giants, which have not yet reached the AGB stage and are observed at the RGB, have low masses $\mathcal{M} < 2.5\mathcal{M}_{\odot}$. As a mechanism for Li production Romano et al. [49] suggest the “cool bottom process”, which is based on the production of beryllium, its dredge-up toward the base of the convective envelope, and subsequent decay down to lithium nuclei in the subsurface layers of the star. Here it is appropriate to cite the recent paper by Jasniewicz et al. 50, who determined $\varepsilon(\text{Li})$ for a sample of solar metallicity G–K giants and subgiants, and found that the highest $\varepsilon(\text{Li})$ is achieved for fast rotating stars ($V \sin i \geq 30 \text{ km/s}$). However, as we pointed out above, spectral features in the form of emissions prevent us from adopting the red-giant status for the star under study.

In conclusion, we have to admit that the evolution stage of V2324 Cyg remains unclear despite the extensive amount of the data that we obtained. On the IR colour–colour diagram IRAS 20572+4919 lies in domain IV populated by planetary and protoplanetary nebulae. According to chronological sequences of Lewis [51], the lack of maser emission in the OH and H₂O bands [31] suggests that the system must be approaching the stage of planetary nebula. This fact agrees with the conclusions of Garcia-Lario et al. [1] and Arkhipova et al. [11] who consider V2324 Cyg as a post-AGB star. However, the post-AGB stage is inconsistent with a number of properties of the star found as a result of our research, first and foremost, the low luminosity of the star: spectral classification points to luminosity class III. Here to the point to recall the paper [15], where the classification of the IRAS 20572+4919 source as a “post-AGB” star is considered as tentative.

The H α profile and very high wind velocity, which are usually found in supergiants, are also inconsistent with the post-AGB status. We see the prospects for further refinement of the distance, mass, and nature of V2324 Cyg to be found in gathering data not only about the object itself, but also about stars seen in the direction of the Cas OB7 association.

4. Conclusions

We performed high-resolution optical spectroscopy of the V2324 Cyg variable star – an optical counterpart of the IR source IRAS 20572+4919. We identified more than 200 absorptions within the wavelength interval 4549–7880 Å (these are mostly Fe II, Ti II, Cr II, Y II, Ba II, and Y II lines) and determined the spectral type and rotation velocity of the star to be F0 III and $V \sin i = 69 \text{ km/s}$, respectively. The main peculiarity of the spectrum of the star are complex P Cyg-type profiles of the H α and Na I D lines.

We analyzed 9 spectra taken in different years (1995–2006) and failed to find either systematic trend of radial velocity V_r with line depth R_{\odot} , or temporal variability of V_r . This result allowed us to adopt the mean value $V_r = -16.8 \pm 0.6 \text{ km/s}$ as the systemic velocity, $V_{\text{sys}} \approx -17 \text{ km/s}$. We found velocities ranging from -140 to -225 km/s (and the expansion velocities from about 120 to 210 km/s for the corresponding layers) from the

velocity to be the highest for the blue component of the H α split absorption: 450 km/s for December 12, 1995.

By the model atmospheres method we determined the effective temperature, $T_{eff}=7500$ K, surface gravity $\log g=2.0$, microturbulence velocity $\xi_t=6.0$ km/s, and metallicity which appear to be equal to solar one. The main peculiarity of the chemical composition of V2324 Cyg is the overabundance of lithium and sodium.

The solar metallicity of the star combined with $V_{sys} \approx -17$ km/s allows us to classify it as an object of the Galactic disk population. Main conclusion of this investigation is the uncertainty of the evolutionary status of V2324 Cyg. Its properties are not entirely consistent with either the post-AGB or RGB stage.

Acknowledgments

We are much indebted to M.V. Yushkin for his assistance in observations and primary data reduction. This work was supported by the Russian Foundation for Basic Research (project 08-02-00072a), the “Extended Objects in the Universe” fundamental research program of the Division of Physical Sciences of the Russian Academy of Sciences, and the “Origin and Evolution of Stars and Galaxies” program of the Presidium of the Russian Academy of Sciences.

References

1. P. Garcia-Lario, A. Manchado, S. R. Pottash, J. Suso and R. Olling. *Astron. & Astrophys. Suppl. Ser.* **82**, 497 (1990)
2. T. Blöcker, *Astrophys. Space Sci.* **275**, 241 (2001)
3. M. Busso, R. Gallino, and G. J. Wasserburg. *Ann. Rev. Astron. & Astrophys.* **37**, 239 (1999)
4. V. G. Klochkova. *MNRAS* **272**, 710 (1995)
5. V. G. Klochkova. *Bull. Spec. Astrophys. Observ.*, **44**, 5 (1997)
6. L. Decin, H. Van Winckel, C. Waelkens, and E. J. Bakker. *A&A*, **332**, 928 (1998)
7. V. G. Klochkova and T. Kipper. *Baltic Astron.* **15**, 395 (2006)
8. V. G. Klochkova, V. E. Panchuk, N. S. Tavalzhanskaya. *Astron. Lett.* **28**, 49 (2002)
9. V. G. Klochkova, V. E. Panchuk, E. L. Chentsov, & M. V. Yushkin. *Astrophys. Bull.* **62**, 217 (2007)
10. V. P. Arkhipova, N. P. Ikonnikova. *Astron. Lett.* **20**, 603 (1994)
11. V. P. Arkhipova, N. P. Ikonnikova, R. I. Noskova, G. V. Sokol. *Astron. Lett.* **26**, 609 (2000)
12. T. M. Gledhill. *MNRAS* **356**, 883 (2005)
13. B. J. Hrivnak, S. Kwok, and T. R. Geballe. *Astrophys. J.* **420**, 783 (1994)
14. D. M. Kelly & B. J. Hrivnak. *Astrophys. J.* **629**, 1040 (2005)
15. P. Garcia-Lario, A. Manchado, W. Ryck, and S. R. Pottash. *Astron. & Astrophys. Suppl.*

16. H. Wishnewski and G. V. Coyne. *Vat. Obs. Publ.* **1**, No 11, 245 (1976)
17. C. B. Pereira and L. F. Miranda, *Astron. & Astrophys.* **462**, 231 (2007)
18. V. E. Panchuk, V. G. Klochkova, I. D. Naidenov, et al., Preprint No. 139 *Spec. Astrophys. Obs. Russian Acad. Sci. (Nizhnij Arkhyz, 1999)*
19. V. E. Panchuk, I. D. Najdenov, and V. G. Klochkova. *Bull. Spec. Astrophys. Observ.* **44**, 127 (1998)
20. V. Panchuk, V. Klochkova, M. Yushkin, and I. D. Najdenov. High resolution echelle spectrograph NES for visible and ground-based UV regions. In: “The UV Universe: stars from birth to death”, *Proceedings of the Joint Discussion No. 4 during the IAU General Assembly of 2006*, Eds. by A. I. Gomez de Castro and M. A. Barstow (2007), p.179.
21. M. V. Yushkin, V. G. Klochkova. Preprint No. 206 *Spec. Astrophys. Obs. Russian Acad. Sci. (Nizhnij Arkhyz, 2005)*
22. G. A. Galazutdinov. Preprint No. 92 *Spec. Astrophys. Obs. Russian Acad. Sci. (Nizhnij Arkhyz, 1992)*
23. G. H. Jacoby, D. A. Hunter, and C. A. Christian. *Astrophys. J. Suppl. Ser.* **56**, 257 (1984)
24. R. O. Gray and R. E. Garrison. *Astrophys. J. Suppl. Ser.* **69**, 301 (1989)
25. Ph. Prugniel and C. Soubiran. *astro-ph/0409214* (2004)
26. Ph. Prugniel, C. Soubiran, M. Koleva, and D. Le Borgne, *astro-ph/0703658* (2007)
27. E. Solano and J. Fernley. *Astron. & Astrophys. Suppl. Ser.* **122** 131 (1997)
28. V. G. Klochkova, G. Zhao, V. E. Panchuk, and S. V. Ermakov. *Chinese J. Astron. & Astrophys.* **4** 279, (2004)
29. R. Faraggiana, M. Gerbaldi, C. van’t Veer, & M. Floquet. *Astron. & Astrophys.* **201**, 259 (1988)
30. B. J. Hrivnak and J. H. Bjeging. *Astrophys. J.* **624**, 331 (2005)
31. O. Suárez, J. F. Gómez, and O. Morata. *Astron. & Astrophys.* **467**, 1085 (2007)
32. D. Shulyak, V. Tsymbal, T. Ryabchikova, Ch. Stütz, W. W. Weiss. *Astron. & Astrophys.* **428** 993 (2004)
33. N. E. Piskunov, F. Kupka, T. A. Ryabchikova, W. W. Weiss, C. S. Jeffery. *Astron. & Astrophys. Suppl. Ser.* **112**, 525 (1995)
34. F. Kupka, N. E. Piskunov, T. A. Ryabchikova, et al., *Astron. & Astrophys. Suppl. Ser.* **138**, 119 (1999)
35. M. Asplund, N. Grevesse, and A. J. Sauval. *ASP Conf. Ser.* **336**, 25 (2005)
36. Y. Takeda and M. Takada-Hidai. *Publ. Astron. Soc. Jap.* **46**, 395, (1994)
37. Y. Takeda, G. Zhao, M. Takada-Hidai, Y.-Q. Chen, Y.-J. Saito, H.-W. Zhang. *Chin. J. Astron. & Astrophys.* **3**, 316, (2003)

39. F. Herwig & S. M. Austin. *Astrophys. J.* **613**, L73 (2004)
40. F. Herwig. *Astron. & Astrophys.* **360**, 952 (2000)
41. C. Sneden, R. G. Gratton & D. A. Crocker. *Astron. & Astrophys.* **246**, 354 (1991)
42. A. Arellano Ferro, S. Giridhar, and P. Mathias. *Astron. & Astrophys.* **368**, 250 (2001)
43. H. van Reyniers and H. Van Winckel. *Astron. & Astrophys.* **365**, 465 (2001)
44. V. G. Klochkova, E. L. Chentsov, V. E. Panchuk, and M. V. Yushkin. *IBVS No. 5584* (2004)
45. V. G. Klochkova, E. L. Chenstov, N. S. Tavalzhanskaya. V. E. Panchuk. *Astron. Rep.* **51**, 642 (2007)
46. J. Brand and L. Blitz. *Astron. & Astrophys.* **275**, 67 (1993)
47. R. M. Humphreys. *Astrophys. J. Suppl. Ser* **38**, 309 (1978)
48. O. Straniero, R. Gallino & S. Cristallo. *Nuclear Physics*, **777**, 311 (2005)
49. D. Romano, F. Matteucci, P. Ventura & F. D` Antona. *Astron. & Astrophys.* **374**, 646 (2001)
50. G. Jasiewicz, A. Recio-Blanco, P. de Laverny, et al., *Astron. & Astrophys.* **453**, 717 (2006)
51. B. M. Lewis. *Astrophys. J.* **338**, 234 (1989)

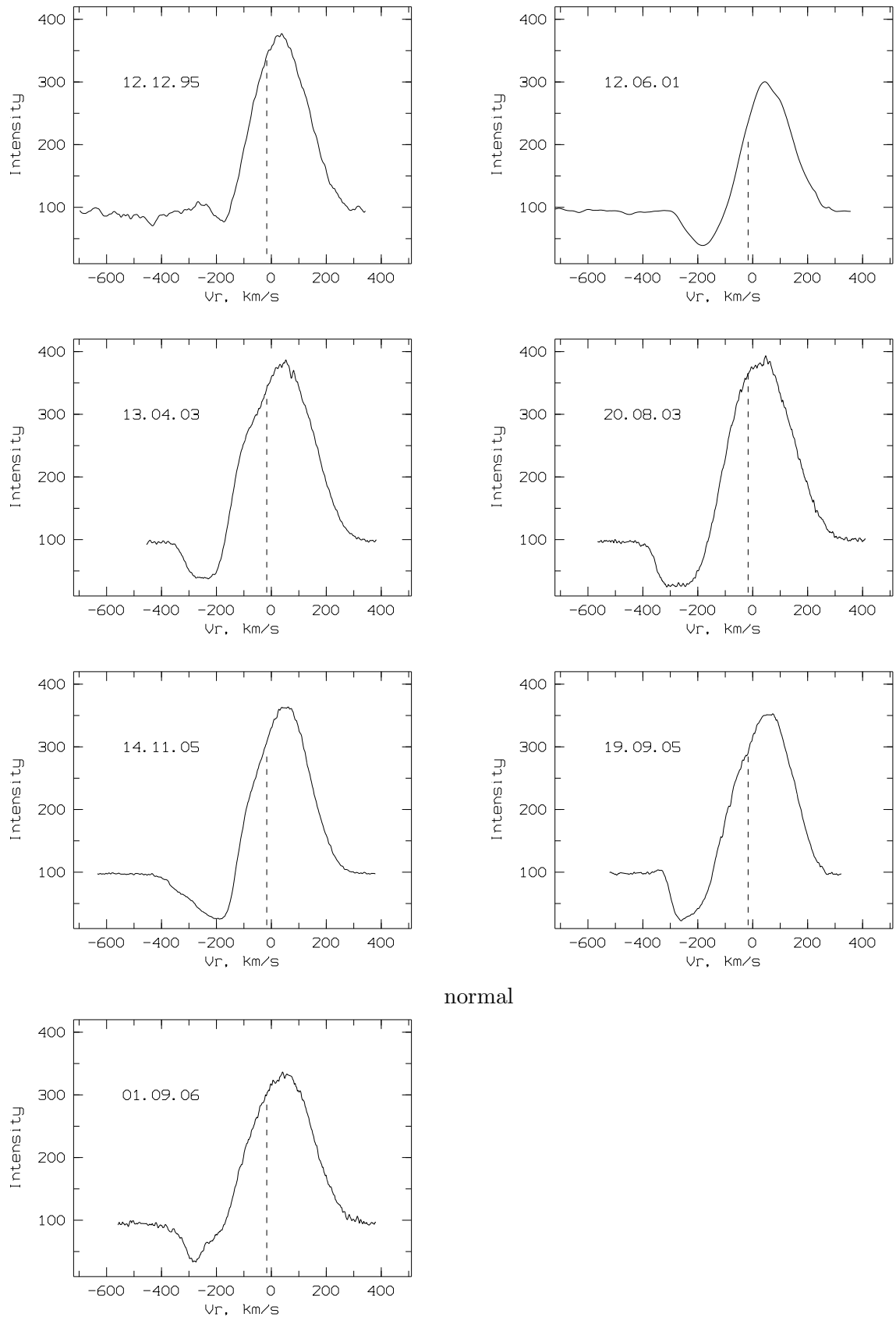


Figure 1. $H\alpha$ -profile variability in the spectra of V2324 Cyg. The dashed line shows the

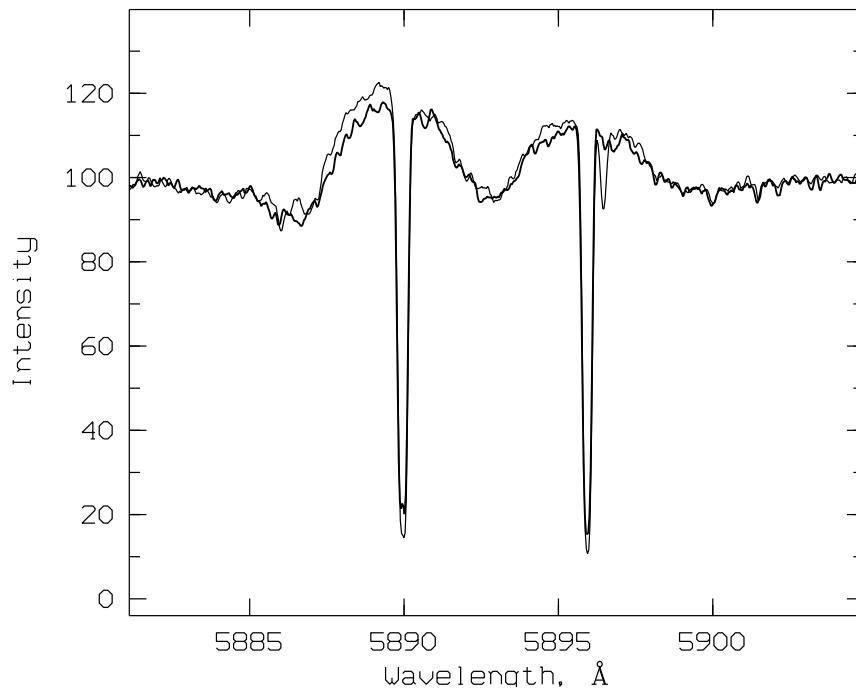


Figure 2. The profile of NaI D lines in two spectra of V2324 Cyg taken in 2005

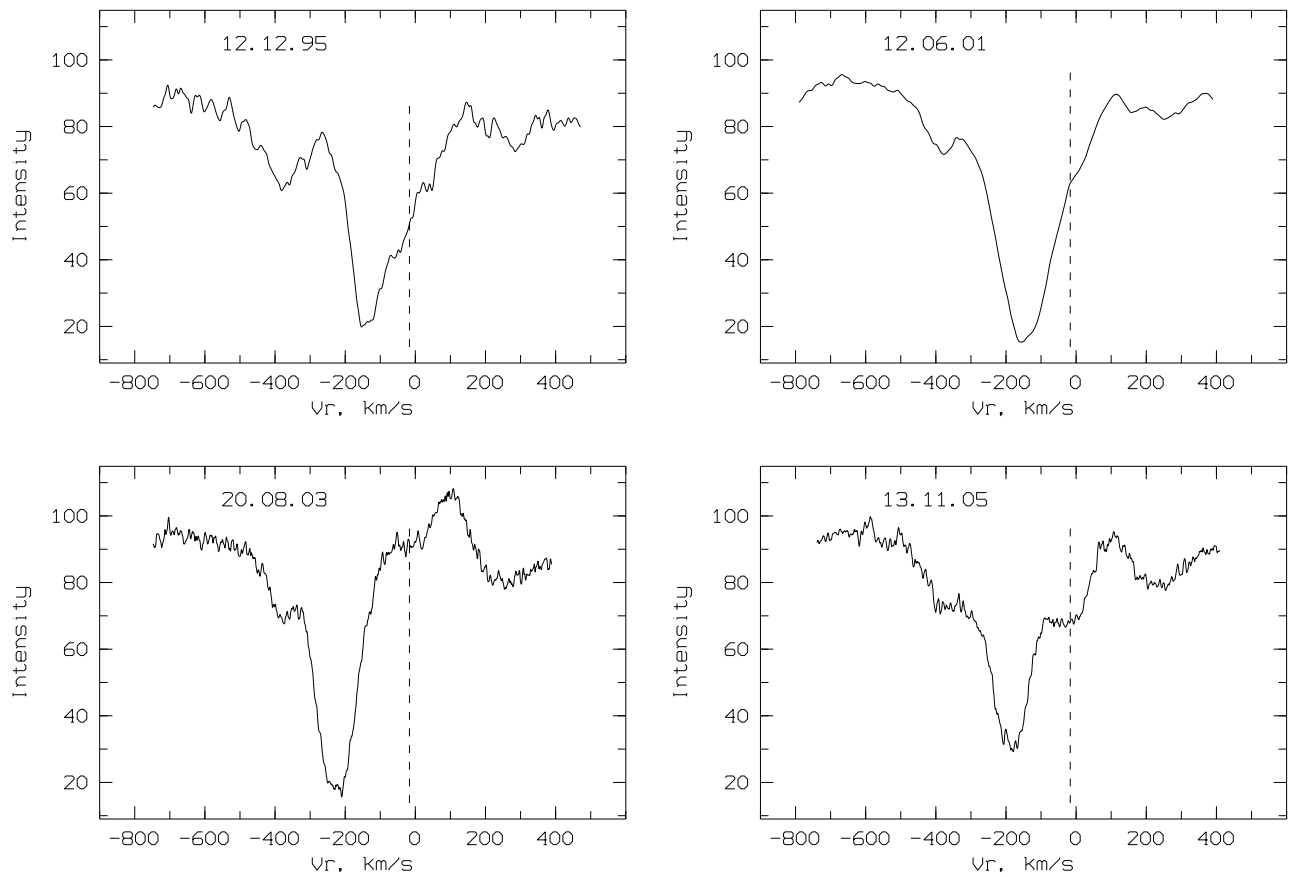


Figure 3. $H\beta$ -profile variability in the spectra of V2324 Cyg. The dashed line shows the mean velocity averaged over photospheric metal lines.

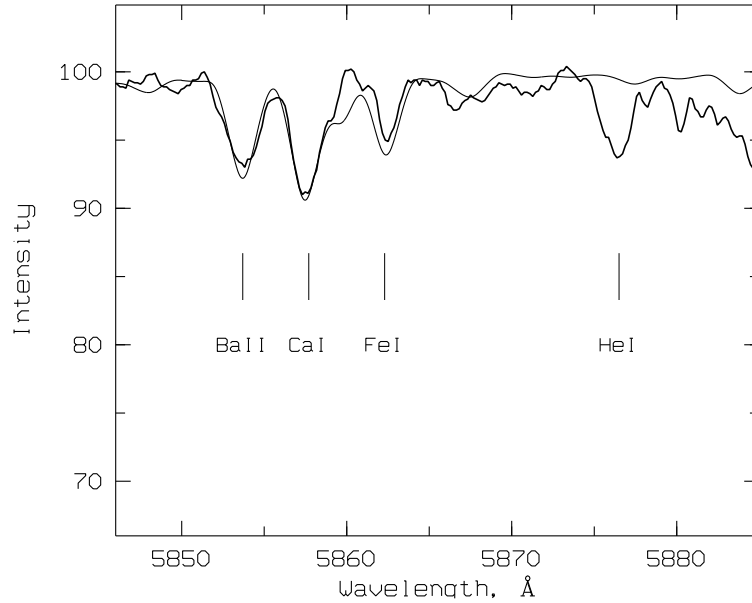


Figure 4. Ba II λ 5853 and He I λ 5876 lines in the spectrum of V2324 Cyg taken in 2001. The thin line represents the theoretical spectrum computed for $T_{eff} = 7500$ K, $\log g = 2.0$, and $\xi_t = 6.0$ km/s and solar elemental abundances.

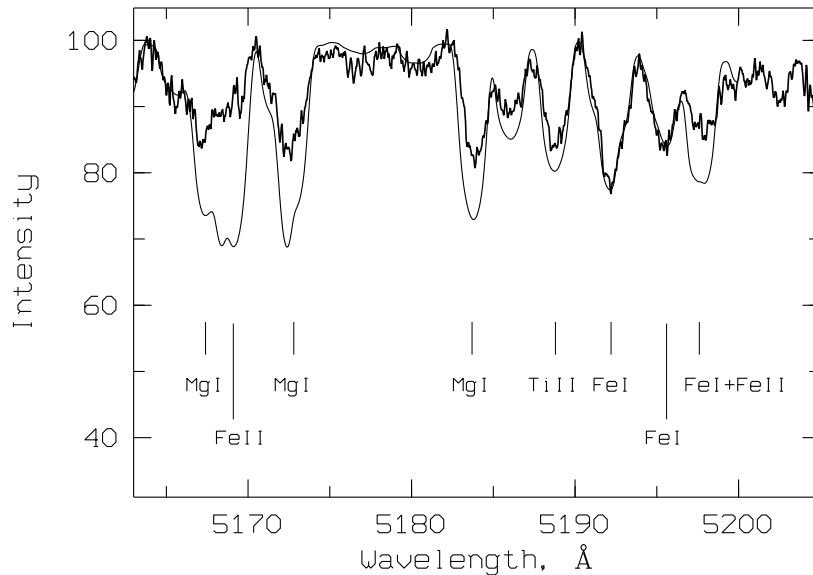


Figure 5. Mg I λ 5167–5183 magnesium triplet and Fe II λ 5169 iron lines in the spectrum of V2324 Cyg taken on November 13, 2005. The thin line represents the theoretical spectrum computed for $T_{eff} = 7500$ K, $\log g = 2.0$, and $\xi_t = 6.0$ km/s and solar elemental abundances.

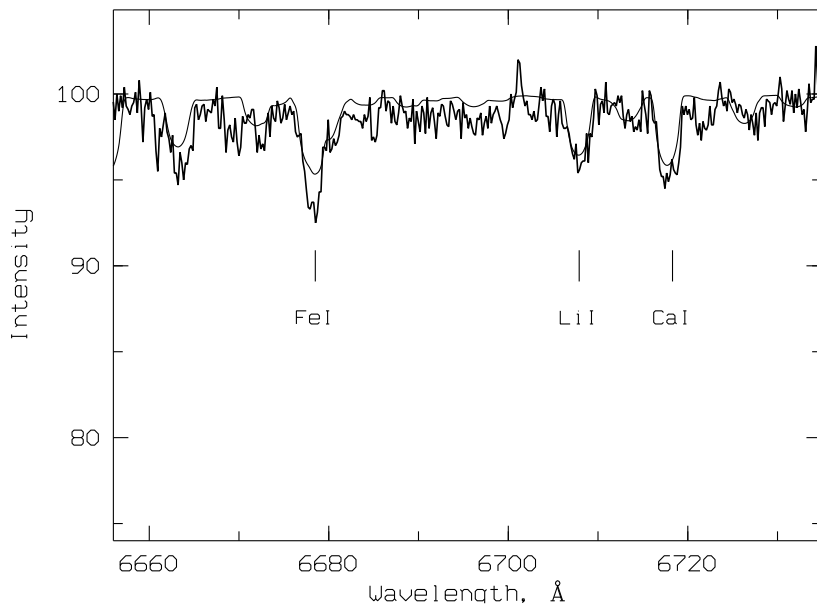


Figure 6. The Li I λ 6707 Å line in the spectrum of V2324 Cyg taken on June 12, 2001. The thin line shows the theoretical spectrum computed for $T_{eff} = 7500$ K, $\log g = 2.0$, and $\xi_t = 6.0$ km/s and the elemental abundances from Table 4.

Table 1. Log of observations of V2324 Cyg made at the 6-m telescope

Date	UT	ΔT , s	$\Delta\lambda$, Å	Spectrograph
12.12.95	16:24	6400	4720–6857	Lynx
12.06.01	23:50	6000	4546–7880	PFES
14.04.03	23:14	16200	5275–6760	NES
15.08.03	21:26	10800	5275–6760	NES
20.08.03	23:54	9600	4519–5997	NES
19.09.05	16:29	12000	5275–6760	NES
13.11.05	16:29	10800	4558–6010	NES
14.11.05	16:40	10800	5275–6760	NES
01.09.06	20:41	2400	5275–6760	NES

Table 2. Residual intensities r and heliocentric radial velocities V_r for selected lines in the spectrum of V2324Cyg. The colon indicates uncertain values

Line	λ , Å	r	V_r , km/s	Date
FeII(38)	4576.34	0.86	−15	
FeII(38)	4583.84	0.83:	−18	
CaI(23)	4585.87	0.88	−15	
CrII(44)	4588.20	0.89	−20	
TiII(50)	4589.95	0.88	−16	
FeI(39)	4602.94	0.90	−	
FeI(554)	4607.65	0.92:	−	
FeI(554)	4613.28:	0.88	−	
CrI(21)				
FeII(37)	4629.33	0.85	−15:	
FeI(115)				
CrII(44)	4634.07	0.89	−15	
FeI(820)	4643.47	0.94	−	
FeI(38)	4654.56:	0.87	−18:	
FeI(554)				
FeII(25)				
ScII(24)	4670.30:	0.86	−	
FeI(821)	4678.85	0.87	−	
MgI(11)	4702.99	0.82	−15	
NiII(98)	4714.42	0.87	−17	
FeII(43)	4731.47	0.86	−	
FeI(38)	4733.60	0.92	−	
FeI(554)	4736.78	0.86	−16	
TiII(92)	4778.99	0.85	−18	
MnI(16)	4783.42	0.87	−16	
TiII(92)	4805.09	0.88	−17:	
ZnI(2)	4810.54	0.95:	−16:	
MnI(16)	4823.52	0.79	−	
CrII(30)	4824.14			
NiI(131)	4829.03	0.93:	−	
CrI(31)	4829.37			
CrII(30)	4836.23	0.90	−	
CrII(30)	4848.25	0.84	−	
H β	4861.33	0.20:	−138:	12.12.95
		0.15	−145	12.06.01
		0.19	−226	20.08.03
		0.30	−182	13.11.05
1	2	3	4	5

Line	λ , Å	r	V_r , km/s	Date
FeI(318)	4871.70:	0.74	—	
FeI(318)	4891.10:	0.75	—	
BaII(3)				
YII(22)	4900.10:	0.86	−18:	
FeI(318)	4903.31	0.87	—	
FeI(318)	4918.90:	0.81	—	
FeI(318)	4920.50	0.80	−16	
FeII(42)	4923.92	0.88	—	
FeI(114)	4924.77			
FeI(1065)				
BaII(1)	4934.00:	0.78	—	
FeI(687)	4950.11	0.94	−20:	
FeI(318)	4957.50:	0.73	—	
FeI(687)	4966.09	0.91	−20:	
FeI(984)	4973.11	0.95	−16:	
FeI(1066)	4988.98:	0.94:	—	
NiI(111)	5017.58			
FeII(42)	5018.40:	0.85	—	
NiI(38)	5020.03	0.90:	—	
ScII(23)	5031.02	0.89	−15	
FeI(383)	5068.80:	0.88	—	
FeI(1094)	5074.75	0.88	−16	
YII(20)	5087.42	0.90	−15	
FeI(1090)	5090.78	0.93	−18	
FeI(16)	5107.55:	0.87	—	
FeI(36)				
NiI(177)	5115.40	0.94:	—	
TiII(86)	5129.16:	0.87	−17:	
FeI(1092)	5133.69	0.88	−20	
FeI(383)	5139.37:	0.82	−17:	
TiII(70)	5154.07:	0.86:	—	
FeI(1089)	5162.27	0.89	−21:	
FeI(1)	5166.28			
MgI(2)	5167.32:	0.83:	—	
FeI(37)	5167.49			
FeI(1)	5168.90			
FeII(42)	5169.03	0.89	−25:	
MgI(2)	5172.68	0.85	−25:	
MgI(2)	5183.61	0.83	−13	
TiII(86)	5185.91	0.90	−18	
TiII(70)	5188.69	0.83	−18:	
CaI(49)	5188.84			
1	2	3	4	5

Line	λ , Å	r	V_r , km/s	Date
FeII(49)	5197.58	0.87	−20:	
FeI(66)	5198.72			
FeI(66)	5202.34	0.91	−17	
CrI(7)	5208.44	0.84	−	
FeI(553)	5208.60			
FeI(553)	5229.85	0.91	−19	
CrII(43)	5232.50			
FeI(383)	5232.94	0.85	−	
CrII(43)	5237.32	0.89	−19	
ScII(26)	5239.82	0.93	−17	
FeI(1)	5247.06			
CrI(18)	5247.57	0.93:	−	
FeI(1)	5250.22			
FeI(66)	5250.65	0.91:	−	
FeI(553)	5273.28:	0.88:	−	
FeI(114)				
FeI(383)	5281.79	0.89	−	
FeI(929)	5288.53	0.96:	−19:	
FeI(553)	5302.31	0.91	−18	
CrII(43)	5310.69	0.96	−15:	
CrII(43)	5313.58	0.94	−17	
FeII(49)	5316.66:	0.87	−16:	
FeII(48)				
FeI(553)	5324.18	0.87	−	
CrI(18)	5345.80	0.93:	−	
CrII(24)	5346.08			
FeII(48)	5362.86	0.90	−18	
FeI(1146)	5364.87	0.89:	−	
FeI(786)	5365.40			
FeI(1146)	5367.47	0.90	−16	
FeI(1146)	5383.37	0.89	−17	
FeI(553)	5393.17	0.91	−18	
FeI(15)	5397.13	0.89	−16:	
FeI(1145)	5398.29			
FeI(1145)	5400.51:	0.93:	−	
FeII(48)	5414.07			
FeI(1165)	5415.20	0.89	−	
TiII(69)	5418.77	0.92	−16	
FeI(1146)	5424.07	0.86	−	
FeII(49)	5425.25			
FeI(15)	5429.70	0.86	−16	
FeI(15)	5434.52	0.89	−16	
1	2	3	4	5

Line	λ , Å	r	V_r , km/s	Date
TiI(3)	5446.59			
FeI(15)	5446.92:	0.83:	-17:	
FeI(1145)				
FeI(15)	5455.56:	0.83	-17:	
FeI(15)	5497.52	0.91	-17	
FeI(15)	5506.79	0.91	-	
DIB	5512.64	0.92	-	
CaI(48)	5512.99			
ScII(31)	5526.81	0.91:	-	
MgI(9)	5528.41	0.87	-	
FeII(55)	5534.84	0.87:	-	
FeI(626)	5535.42			
FeI(1183)	5554.90	0.94	-	
FeI(1183)	5565.71	0.95	-15	
FeI(686)	5569.62	0.93	-15	
FeI(686)	5572.86:	0.90	-16:	
FeI(686)	5576.10	0.94	-18:	
CaI(21)	5581.98	0.93	-17	
CaI(21)	5594.48:	0.88	-18:	
FeI(1182)	5594.66			
CaI(21)	5601.28	0.92:	-	
CaI(21)				
FeI(686)	5602.90:	0.88	-	
FeI(209)	5615.31			
FeI(686)	5615.60:	0.86	-17:	
FeI(1314)	5633.95	0.96:	-15:	
FeI(1183)	5679.03	0.96	-18	
NaI(6)	5688.21	0.93:	-	
NiI(231)	5715.09	0.97:	-	
FeI(1107)	5717.84	0.97:	-16:	
FeI(1087)	5731.77	0.95:	-15:	
FeI(1107)	5763.00:	0.92:	-17:	
SiI(17)	5772.15	0.96	-16	
FeI(1087)	5775.08	0.98:	-	
DIB	5780.37	0.90	-7:	
DIB	5796.96	0.87	-8	
FeI(1179)	5816.38	0.95:	-16:	
DIB	5849.80	0.96	-8	
BaII(2)	5853.68	0.92	-16	
CaI(47)	5857.45	0.91	-	
NiI(228)	5857.75			
FeI(1181)	5859.59	0.95:	-	
1	2	3	4	5

Line	λ , Å	r	V_r , km/s	Date
FeI(1180)	5862.36	0.95	−15:	
NaI(1)	5889.95	0.82/1.17	−140/2:	12.12.95
		0.90/1.10	−160/−8:	12.06.01
		0.90/1.22	−220/−21:	14.04.03
		0.96/1.23	−207/−18:	15.08.03
		0.84/1.20	−210/−22:	20.08.03
		0.81/1.24	−181/−25:	19.09.05
		0.90/1.20	−188/−26:	14.11.05
		0.90/1.20	−200/−16:	1.09.06
NaI(1) I.S.		0.07	−13	
NaI(1)	5895.92	0.88/1.09	−137/−2:	12.12.95
		0.93/1.08	−150/−15:	12.06.01
		1.02/1.19	−169/−20:	14.04.03
		1.05/1.18	−172/−37:	15.08.03
		0.98/1.16:	−180/−37:	20.08.03
		0.90/1.17	−164/−20:	19.09.05
		0.94/1.12	−168/−18:	14.11.05
		0.95/1.12	−150/−37:	1.09.06
NaI(1) I.S.		0.07	−13	
FeI(1180)	5914.17:	0.94:	−16:	
FeI(1181)				
FeI(1260)	5987.07	0.96:	—	
FeII(46)	5991.37	0.95	−17:	
FeI(959)	6003.02	0.97:	−15:	
MnI(27)	6016.64	0.97	−15:	
FeI(1178)	6024.07	0.95	−14:	
FeI	6042.10	0.96	−17:	
FeI(1259)	6056.01	0.96	−16:	
FeI(207)	6065.49	0.93	−17:	
FeII(46)	6084.10	0.97:	—	
FeI(1259)	6102.18			
CaI(3)	6102.73:	0.87	−16:	
FeI(1260)	6103.19			
CaI(3)	6122.22	0.89	−17	
FeI(169)	6136.62			
FeI(62)	6137.00	0.87:	—	
FeI(207)	6137.70			
BaII(2)	6141.72	0.86	−17	
FeII(74)	6147.74	0.93	—	
FeII(74)	6149.25			
CaI(20)	6161.29			
1	2	3	4	5

Line	λ , Å	r	V_r , km/s	Date
CaI(3)	6162.18:	0.89	−18:	
DIB	6195.96	0.94	−11	
FeI(207)	6200.32	0.97	—	
DIB	6203.08	0.96	−12:	
FeI(207)	6230.73	0.92	−17	
FeI(62)	6265.14	0.96:	—	
SiII(2)	6347.10	0.90	−14:	
SiII(2)	6371.36	0.93	—	
DIB	6379.29	0.91	−12	
FeI(168)	6393.61	0.93	−16	
FeI(816)	6400.01:	0.91	−17:	
FeI(13)	6400.32			
FeI(816)	6411.66	0.95	−16:	
CaI(18)	6439.08	0.89	−17	
CaI(19)	6449.82	0.92	−18:	
CaI(19)	6455.60			
FeII(74)	6456.39:	0.88	−16:	
CaI(18)	6462.61:	0.90	−16:	
FeI(168)	6462.73			
FeI(268)	6546.25	0.91	−15	
H α	6562.81	0.77/3.70:	−180/31	12.12.95
		0.40/3.00:	−183/47	12.06.01
		0.40/3.90	−247/45	14.04.03
		0.29/3.90	−278/30	15.08.03
		0.24/3.60	−260/42	19.09.05
		0.25/3.60	−195/51	14.11.05
		0.35/3.30	−280/40	1.09.06
DIB	6613.56	0.87	−12:	
NiI(43)	6643.64	0.96	−13:	
DIB	6660.64	0.95:	−10:	
FeI(268)	6678.00	0.94	−14:	
LiI(1)	6707.80:	0.95	−15:	
CaI(32)	6717.69	0.94	−17	
CaI(30)	7148.16	0.89:	—	
FeI(1077)	7495.08	0.93	−15:	
FeI(1077)	7511.03	0.94	—	
NiI(187)	7555.61	0.95	—	
FeI(1077)	7568.91	0.94	—	
FeI(1306)	7742.72	0.94	—	
OI(1)	7771.94	0.96:	−16:	
OI(1)	7774.17	0.90:	—	
OI(1)	7775.39			
1	2	3	4	5

Line	λ , Å	r	V_r , km/s	Date
FeI(1154)	7780.57	0.93	−15:	
FeI(1154)	7832.21	0.93:	−	
1	2	3	4	5

Table 3. Uncertainty $\Delta \log \varepsilon(X)$ of elemental abundances in the atmosphere of V2324 Cyg due to the errors of the parameters of the star atmosphere

X	ΔT_{eff} +200 K	$\Delta \log g$ +0.5	$\Delta \xi_t$ -1.0 km/s
HeI	-0.57	-0.04	+0.08
LiI	+0.07	-0.06	+0.02
Cl	-0.02	+0.03	+0.05
OI	-0.10	+0.09	+0.01
NaI	+0.02	-0.07	+0.04
MgI	-0.12	-0.24	+0.27
SiI	-0.14	+0.09	+0.07
SI	+0.02	-0.02	+0.03
CaI	-0.04	+0.07	+0.02
ScII	-0.03	+0.13	+0.04
TiII	+0.00	+0.14	+0.09
CrI	+0.06	-0.05	+0.09
CrII	-0.01	+0.13	+0.04
FeI	+0.03	-0.05	+0.14
FeII	-0.02	+0.14	+0.13
NiI	+0.04	-0.06	+0.05
ZnI	+0.06	-0.04	+0.04
YII	+0.03	+0.27	+0.07
BaII	+0.06	+0.04	+0.29

Table 4. Abundances $\varepsilon(X)$ of elements in the atmosphere of V2324 Cyg. Here σ is the standard deviation of the abundance and “n”, the number of lines used in the computation. The computation was performed with the model-atmosphere parameters $T_{eff}=7500$ K, $\log g=2.0$, and $\xi_t=6.0$ km/s. The elemental abundances for the solar atmosphere are adopted from [35]

The Sun		V2324 Cyg			
X	$\varepsilon(X)$	$\varepsilon(X)$	σ	n	[X/Fe]
LiI	3.25 ¹	≥ 3.93		1	$\geq +0.68$
Cl	8.39	8.73	0.08	9	+0.35
OI	8.66	8.53	0.28	3	-0.12
NaI	6.17	7.20	0.22	3	+1.04
MgI	7.53	7.96	0.04	2	+0.43
SiII	7.51	7.22	0.09	5	-0.28
Si	7.11	7.41	0.19	2	+0.31
CaII	6.31	6.85	0.13	4	+0.55
ScII	3.05	3.05	0.15	8	+0.01
TiII	4.90	4.76	0.08	11	-0.13
CrI	5.64	5.39	0.10	5	-0.24
CrII		5.31	0.06	19	-0.32
FeI	7.45	7.44	0.07	28	+0.00
FeII		7.43	0.10	14	-0.01
NiI	6.23	6.23	0.10	8	+0.01
ZnI	4.60	4.68	0.17	2	+0.09
YII	2.21	2.18	0.27	2	-0.02
BaII	2.17	2.64	0.09	4	+0.46

Remark: 1—the value for meteorites [35]

Table 5. Equivalent widths W_λ of interstellar NaID lines and DIBs. Approximate estimates are given for the equivalent widths of NaID lines because of the complex shapes of their profiles (see Fig. 2)

Spectral feature	W_λ , Å
D2 5889	≈ 0.40
D1 5895	≈ 0.37
DIB 5512	0.08
DIB 5780	0.23
DIB 5797	0.13
DIB 5850	0.03
DIB 6196	0.04
DIB 6203	0.04
DIB 6379	0.07
DIB 6614	0.12
DIB 6661	0.03